Analyst

PAPER

Cite this: DOI: 10.1039/c4an00064a

IR action spectroscopy shows competitive oxazolone and diketopiperazine formation in peptides depends on peptide length and identity of terminal residue in the departing fragment†

L. J. Morrison,[a] J. Chamot-Rooke[b] and V. H. Wysocki*[a]

Received 10th January 2014
Accepted 26th February 2014

DOI: 10.1039/c4an00064a

www.rsc.org/analyst

The interplay between the entropically and enthalpically favored products of peptide fragmentation is probed using a combined experimental and theoretical approach. These b_2 ion products can take either an oxazolone or diketopiperazine structure. Cleavage after the second amide bond is often a favorable process because the products are small ring structures that are particularly stable. These structures are structurally characterized by action IRMPD spectroscopy and semi-quantified using gas-phase hydrogen–deuterium exchange. The formation of the oxazolone and diketopiperazine has been thought to be largely governed by the *identity* of the first two residues at the N-terminus of the peptide. We show here that the length of the precursor peptide and identity of the *third* residue play a significant role in the formation of the diketopiperazine structure in peptides containing an N-terminal asparagine residue. This is additionally the first instance showing an N-terminal residue with an amide side chain can promote formation of the diketopiperazine b_2 ion structure.

Introduction

Mass spectrometry and tandem mass spectroscopy have gained increasing popularity as proteomics and structural biology tools in recent years. With the development of soft ionization techniques such as electrospray and nanospray ionization and the ongoing development of different fragmentation techniques, the characterization of protein primary and quaternary structure by tandem mass spectrometry has become increasingly prevalent.[1–9] Collision induced dissociation, or CID, is perhaps the oldest and perhaps most well established of these methods, with extensive studies examining the enthalpic and entropic factors that define fragmentation in small peptide and non-peptide molecules. One of the principles on which this work is based is known as Rice–Ramsperger–Kassel–Marcus (RRKM) theory, which utilizes both experimental and theoretical data to estimate unimolecular reaction rates.[10] However, this simplistic model fails for large biomolecular systems, as the time scale predicted for the fragmentation of a large protein by RRKM theory far exceeds the analysis time of such a protein in a typical time-of-flight mass spectrometer.[11] Thus, a deeper understanding of the energetics of peptide fragmentation in systems of increasing size is needed to understand the fragmentation behavior of peptides and proteins in mass spectrometry. Here, we utilize a penta-peptide scaffold and the well-studied fragmentation to the b_2 fragment to experimentally probe the interplay between entropic and enthalpic factors in the fragmentation behavior of peptides.

The standard fragmentation pathway of protonated peptides by CID occurs at the backbone amide bond, generating a series of "b" and "y" type ions, wherein the C-terminal fragment or y ion is a truncated peptide and the N-terminal portion forms a cyclic structure. The smallest b ion, the b_2, is composed of two residues and can form either an oxazolone or a diketopiperazine structure. Both structures are formed by nucleophilic attack on the amide carbonyl carbon of the second peptide linkage, with the preceding carbonyl oxygen acting as the nucleophile in the oxazolone pathway and the N-terminus of the peptide acting as the nucleophile in the diketopiperazine pathway.[12,13] The diketopiperazine pathway also requires an isomerization step in which the first amide bond isomerizes from a *trans* configuration to a *cis* configuration prior to ring closure. This isomerization step adds an interesting chemical aspect to the formation of b_2 ions: although the diketopiperazine is typically thermodynamically more stable, *trans–cis* isomerization adds a kinetic barrier to the formation of this structure.[14,15] The typical result is an interplay in which either the thermodynamic (diketopiperazine) or the kinetic product (oxazolone) is formed, although the kinetic pathway is typically preferred in CID experiments.[16–19]

[a]*Department of Chemistry and Biochemistry, The Ohio State University, 484 W. 12th Ave, Columbus, OH 43210, USA. E-mail: wysocki.11@osu.edu*

[b]*Pasteur Institute, 28 Rue du Docteur Roux, 75724 PARIS Cedex 15, France*

† Electronic supplementary information (ESI) available. See DOI: 10.1039/c4an00064a

A number of studies have shown that residue identity plays an influential role in favoring of the oxazolone or diketopiperazine pathways. Histidine containing b_2 systems have been extensively studied, and it has been shown that HA, AH, HG, and GH all form mixtures of diketopiperazine and oxazolone structures while HP forms dominantly diketopiperazine.[13,20,21] Wysocki and coworkers have shown evidence indicating that the diketopiperazine structure is present in low abundance for the AP, IP, and VP systems and have rationalized these findings by suggesting that the known higher cis character of the proline amide bond makes diketopiperazine formation favorable.[22,23] The Polfer lab has recently demonstrated that an arginine residue in the first or second position also makes diketopiperazine formation competitive in b_2-H_2O ions.[24] Although b_2 ions that contain only aliphatic and aromatic residues have been shown to feature exclusively oxazolone structures,[25–27] a basic residue in residue positions 1 or 2 has been shown to allow diketopiperazine formation.[20,24]

In this paper we explore the influence of collision energy on diketopiperazine and oxazolone formation in NAA and NAXIG peptide systems using a combination of energy resolved HDX and action IRMPD spectroscopy. Being only moderately basic, the asparagine side chain cannot sequester the mobile proton as well as a strongly basic residue such as arginine, but can still engage in a number of different proton bridging chemistries as the N-terminal amino acid.[28] The results show that peptide length and bulk in the side chain of the third residue has a strong influence on the structure of the two-residue b_2 fragment that forms following activation by CID.

Experimental

Peptide synthesis

Fluorenylmethyloxycarbonyl chloride (FMOC) protected amino acids were obtained from Novabiochem (San Diego, CA) and peptides were synthesized in-house using standard FMOC solid phase synthesis techniques.[29] The C-terminal, resin-linked residue was used without purification and treated with dimethylformamide (DMF) to swell the polymer bead. The FMOC protecting group was removed from the growing peptide by washing with 70 : 30 DMF–piperidine solvent. Coupling was performed in a stepwise manner using-benzotriazole-*N*,*N*,*N*′,*N*′-tetramethyl-uronium-hexafluoro-phosphate (HBtU) and *N*,*N*-diisopropylethylamine (DIEA) to promote formation of the amide bond. Peptides were cleaved from the resin by incubation in 95% trifluoracetic acid and were extracted twice with diethyl ether. Purified peptides were then diluted into 50 : 50 : 0.1% acetonitrile–H_2O–formic acid electrospray solvent before introduction into the mass spectrometer.

Mass spectrometry and action IRMPD

Deuterated ammonia was used for all gas-phase hydrogen–deuterium exchange (HDX) studies and was obtained from Sigma-Aldrich (St. Louis, MO). Fragmentation and hydrogen–deuterium exchange studies were performed on a Thermo Scientific (Waltham, MA) Velos Pro dual linear ion trap. Following introduction to the gas phase by an electrospray source, precursor ions were monoisotopically mass selected in the high pressure region of the trap and fragmented by higher-energy collisional dissociation (HCD) to generate the b_2 ions. MS^3 was performed by selecting the b_2 ion population and further fragmenting it by HCD.[30] HCD was performed using normalized collision energies ranging between 10 and 20% for MS^3 studies. Thermo Scientific expresses HCD as a relative percentage value and the actual voltages used in the instrument are proprietary and therefore unknown. For this reason, HCD energy will be expressed as a percentage. Gas-phase hydrogen–deuterium exchange (HDX) was performed by saturating the trap with deuterated ammonia and subsequently flushing with helium to generate a low ambient pressure of deuterated ammonia that remained relatively constant for several minutes. The exchange of leucine-enkephalin for 10 ms was used to monitor this pressure and incubation of the analyte b_2 ions was performed in triplicate in all experiments for 2 minute intervals using a deuterated ammonia pressure that resulted in 5% exchange of leucine-enkephalin.

Action IRMPD spectroscopy was performed using a Bruker Esquire 3000+ ion trap coupled to a free electron laser at the CLIO facility in Orsay, France.[31,32] Ions were introduced to the gas phase by electrospray ionization and protonated precursor molecules transmitted to the ion trap for CID and IRMPD. Precursor ions of sequence NAA, and NAXIG (X = alanine (A), aminobutyric acid (Abu), valine (V) and *tert*-butyl glycine (tbG)) were mass selected and fragmented within the ion trap to generate b_2 ions. MS^4 experiments, in which the b_2-NH_3 fragment was irradiated by the FEL laser, were performed by generating the NAAIG b_2 ion by trap CID, isolating it in the trap, and further activating it by trap CID. Once generated, b_2 and b_2-NH_3 ions were isolated respectively, and subjected to 180 ms pulses of irradiation from the free electron laser, with pulses comprised of four, 10 μs macropulses spaced by 40 ms intervals. Each macropulse was composed of 8 micropulses, each lasting one picosecond and spaced by 16 ns intervals. Typical laser powers were 450–600 mW at 1500 cm^{-1}. Irradiation of the laser results in fragmentation of the b_2 or b_2-NH_3 ion if the frequency of the laser is equal to an IR absorption band of the ion. Following irradiation at each frequency, fragment and precursor ions were detected using the ion trap analyzer. Spectra were generated by either plotting the total fragmentation efficiency of the b_2 or b_2-NH_3 ion against irradiation frequency. Because the oxazolone and diketopiperazine structures often fragment differently, fragmentation efficiency can alternatively be considered with regard to a single fragment, giving IRMPD spectra reflecting a single structure if the fragment is unique to the structure. The fragmentation efficiency of the b_2 ion will be presented in some cases by considering separately the b_2-CO and b_2-NH_3 fragments.

Computations

Optimizations and frequency calculations were performed using the Gaussian 09 software package with a B3LYP/6-311++G** basis set.[33] Preliminary conformations of b_2

oxazolone and diketopiperazine structures were obtained using a conformation search function within the Macromodel software package.[34] Collections of conformations were generated for both the diketopiperazine and oxazolone classes of molecules, considering all amine nitrogens, amide oxygens, and the asparagine side chain amide nitrogen as potential protonation sites. Redundant conformers were eliminated at the B3LYP/6-31G level if they shared identical bridging with another conformer and were greater than 50 kJ mol^{-1} higher in energy than the lowest energy conformer. Frequency spectra were scaled by 0.978 and the full-width at half-maximum peak width adjusted to 10 cm^{-1} to best correlate with experimental spectra. The same approach was used for the b_2-NH_3 structures, following formation of the oxazolone or diketopiperazine b_2-NH_3 by the suggested mechanisms shown in ESI, Fig. S1.† Calculations of this type were also performed on AlaAsn succinimide and imino-γ-butyrolactone structures and the energies and frequency spectra associated with these rearranged structures are shown in ESI, Fig. S2.†

Results and discussion

Comparison of the b_2 ion population from NAA, NAAIG, and NAVIG

Peptides featuring an N-terminal asparagine or glutamine have been shown previously by Stein and coworkers to fragment *via* abundant water and ammonia loss pathways.[35,36] The fragmentation behavior of the b_2 ion from NAA, NAAIG, and NAVIG by CID is consistent with their findings (Fig. 1). The b_2 ions from these precursors exhibit largely the same fragments at *m*/*z* 169 (b_2-NH_3), 158 (b_2-CO, a_2), and 141 (b_2-CO-NH_3), representative of two major fragmentation pathways: ammonia loss, CO loss to form the a_2 ion, and a combination of the two. The intensities of the CO loss and ammonia loss fragments differ in each of the three spectra, however, suggesting that the b_2 ions may have different structures. Action IRMPD was therefore used to probe these b_2 ions, with the assumption that mixtures of structures might be present for these b_2 ions.

Action IRMPD spectra were obtained for the b_2 ions from singly charged peptides with sequence NAA, NAAIG, and NAVIG. The b_2 ion action IRMPD spectra from these analogues are shown in Fig. 2(a)–(c). From inspection of the experimental IRMPD spectra from NAA and NAAIG, clear differences in the b_2 absorption behavior are evident in the 1500–2000 cm^{-1} range, suggesting that at least two different structures exist for the NA b_2 ion. These spectra suggest that the type of b_2 ion structure that forms is strongly related to the length of the precursor peptide. Inspection of the action IRMPD spectrum of the b_2 ion from NAVIG shows that it contains features observed in both the NAA and NAAIG experimental b_2 spectra, suggesting the b_2 population from this analogue could be a mixture of the two structures and indicating the influence of the third residue on b_2 ion structure. Dashed red and dashed blue overlays are shown in Fig. 2(c) and were generated by considering only the carbon monoxide loss and ammonia loss peaks from the NAVIG b_2 ion, respectively. The dashed blue trace (ammonia loss) is observed to share the same bands as the action IRMPD spectrum of NAAIG and the dashed red trace agrees very well with the NAA experimental b_2 spectrum. Thus, treatment of the data in this way allows a clear separation of the IRMPD spectra of the two different isomers.

The b_2 population from NAAIG exhibits dominant absorption bands at 1280, 1420, 1600, and 1750 cm^{-1} while the b_2 population from NAA features dominant absorption bands at 1610 and 1690, as well as a weak band at 1925 cm^{-1}. Bands in the relatively high range of approximately 1925 cm^{-1} are typically thought to correspond to a ring carbonyl stretching mode

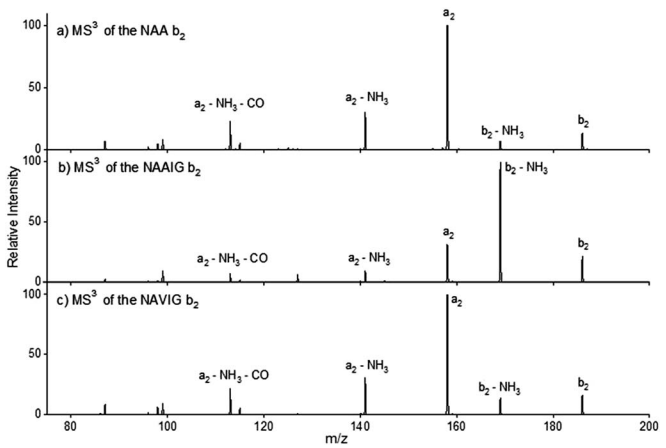

Fig. 1 MS^3 of the b_2 ions of (a) NAA, (b) NAAIG, and (c) NAVIG using HCD to fragment the precursor and the subsequent b_2 ion population, respectively. The b_2 ions of NAVIG and NAAIG were generated using 20% HCD energy and the b_2 ion from NAA was generated using 12.5% HCD energy in order to compensate for its smaller size. The b_2 populations from all precursors were fragmented using 10% HCD collision energies.

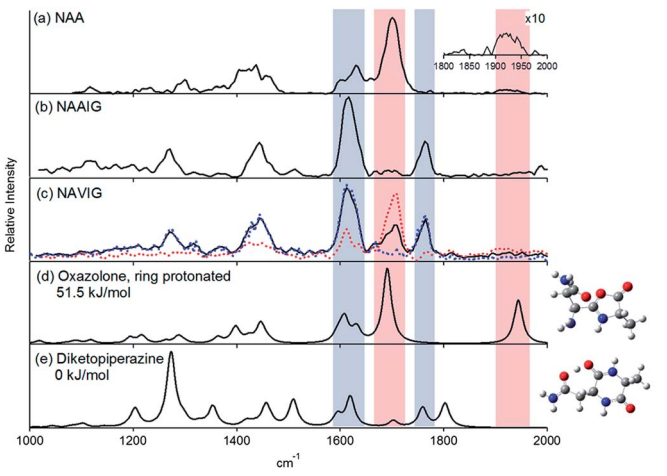

Fig. 2 Experimental action IRMPD spectra of the b_2 populations of (a) NAA, (b) NAAIG, and (c) NAVIG. The theoretical IR spectrum for the ring nitrogen protonated oxazolone is shown in (d) and the theoretical spectrum for the diketopiperazine is shown in (e). Red (maxima at 1610 and 1690 cm^{-1}) and blue (maxima at 1610 and 1750 cm^{-1}) dashed traces in (c) show the action IRMPD spectrum from the b_2 population of NAVIG generated by separately considering the CO loss (red) and NH_3 loss (blue) peaks respectively.

and are often considered diagnostic of an oxazolone structure. Laser power in this range is relatively weak (≈210–250 mW) and this band typically appears lower in intensity than predicted by DFT calculations. Nonetheless, the IRMPD spectrum for the b_2 ion of NAA can be seen to be in excellent agreement with the calculated IR spectrum of the ring protonated oxazolone structure shown in Fig. 2(d). This is in agreement with recent work published by Grzetic and Oomens, in which they also found that the b_2 ion from NAA was an oxazolone structure.[37] Although it is typical for the intensity of peaks in action IRMPD spectra to be quite different than in the predicted IR spectra, the relative intensity of the bands at 1420, 1610, and 1690 cm^{-1} agree very well with theory. The predicted spectrum of the lowest energy diketopiperazine structure, however, is in poorer agreement with the experimental b_2 spectrum from the NAAIG peptide. Higher energy diketopiperazine structures and AlaAsn succinimide and imino-γ-butyrlactone structures also match poorly with the experimental spectrum (see ESI Fig. S2†). Although theory predicts several diketopiperazine vibrational modes at 1450 (ring amide II), 1625 (NH_2 scissor), and 1750 cm^{-1} (ring amide I) that agree relatively well in position with the intense absorption modes observed experimentally, several bands predicted by theory (1200, 1510, and 1800 cm^{-1}) are not observed in the experimental spectrum. Moreover, the intensity of the strong bands in the experimental spectrum does not correlate well with the predicted spectrum. For this reason, it is not possible to confidently assign the b_2 population from NAAIG as a diketopiperazine. Action IRMPD suggests, however, that NAA dominantly forms an oxazolone b_2 ion structure, NAAIG dominantly forms a second b_2 ion structure, and NAVIG forms a mixture of the two.

One reason that theory seems to poorly predict the diketopiperazine structure of the NA b_2 ion is due to the asparagine side chain. Because of its length, it can bridge and stabilize the mobile proton in a variety of different conformations depending on the dihedral angle of the side chain. Small shifts in this angle result in dramatic red and blue shifting of the predicted absorption modes. This effect is also likely related to multiple photons being absorbed in action IRMPD experiments, in which small structural changes, such as the shifting of this side chain, occur following absorption of the first photon. Thus, in order to circumvent multi-photon effects and the influence of the "floppy" side chain, action IRMPD was performed on the b_2-NH_3 fragment from the b_2 of NAAIG. If a diketopiperazine is present as a b_2 structure, nucleophilic attack from the diketopiperazine ring carbonyl oxygen on the side chain amide carbonyl carbon will result in the closure of a five-membered ring and ammonia loss. An analogous pathway is available for the oxazolone structure, in which the ring nitrogen acts as the nucleophile (see ESI, Fig. S1† for the proposed mechanism). The advantage of these two structures is that they are both rigid double ring structures with limited conformational flexibility (see structures in Fig. 3). Because the diketopiperazine and oxazolone structures are not known to interconvert, the b_2-NH_3 structure is a direct reflection of the b_2 population and should confirm whether the diketopiperazine structure is present in the b_2 ion population. The b_2-NH_3 population from NAAIG was generated by fragmenting NAAIG by trap CID in MS^2 and further isolating and fragmenting the b_2 population in MS^3. The experimental action IRMPD spectrum of this b_2-NH_3 population is shown in Fig. 3(a) and the theoretical diketopiperazine-NH_3 and oxazolone-NH_3 are shown in Fig. 3(b) and (c), respectively. The inset of Fig. 3(a) shows the range of 1850–2000 cm^{-1}, which was acquired using a laser power higher than typical in this range (450 mW). From inspection, the agreement between the experimental and the calculated spectra for diketopiperazine b_2-NH_3 can be seen to be very good, with excellent agreement of the amide II mode at 1700 and amide I mode 1790 cm^{-1}. In the high power scan, additional agreement can be seen in the lactone carbonyl vibrational mode that appears at 1990 cm^{-1}. The IRMPD spectrum of the b_2-NH_3 formed from the b_2 of NAAIG confirms that the other structure observed in the b_2 populations of the NAAIG and NAVIG analogues is in fact a diketopiperazine. This is the first example of diketopiperazine formation in systems lacking a basic residue or a proline. Moreover, it is the first evidence to show that peptide length and third residue identity directly influence the b_2 ion structure that forms.

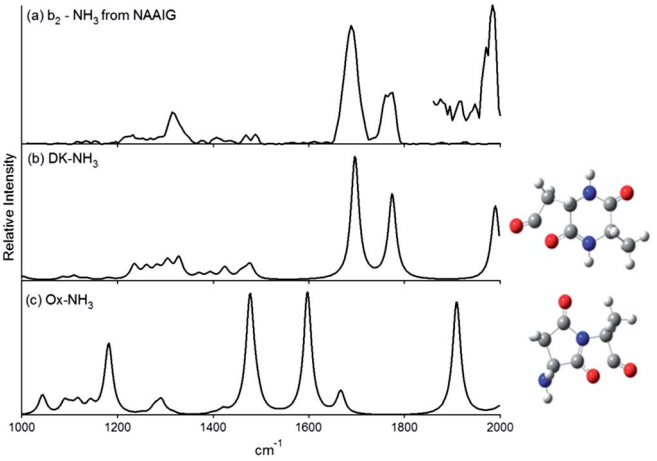

Fig. 3 Experimental action IRMPD spectrum of the b_2-NH_3 from NAAIG is shown in (a), the theoretical IR spectrum of the diketopiperazine-NH_3 is shown in (b), and the theoretical IR spectrum of the oxazolone-NH_3 is shown in (c). The inset in (a) shows the range of 1850–2000 cm^{-1} that was recorded using a higher power of the FEL laser in that range (450 mW).

Examination of the third residue effect: IRMPD and HDX of NAXIG analogues

In order to better understand the role of the third residue on b_2 ion formation, action IRMPD and hydrogen–deuterium exchange (HDX) were performed on the b_2 population from NAXIG pentapeptides, wherein X was 2-aminobutyric acid (Abu) and *tert*-butyl glycine (tbG) in addition to alanine (A) and valine (V). The left panel of Fig. 4 shows the action IRMPD spectra of the b_2 ions from these analogues. As discussed above, the action IRMPD spectrum of the b_2 ion from NAAIG features dominant bands at 1420, 1600, and 1750 cm^{-1} that correspond to the diketopiperazine structure. As the branching chemistry of the

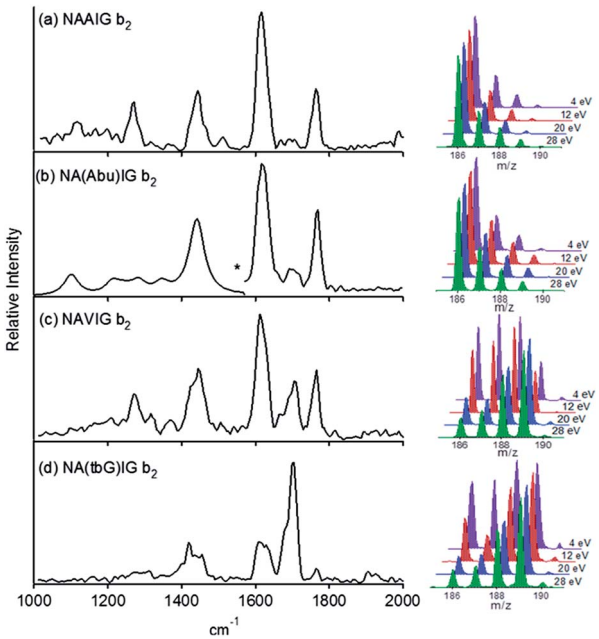

Fig. 4 (Left) action IRMPD of the b_2 population from (a) NAAIG, (b) NA(Abu)IG, (c) NAVIG, and (d) NA(tbG)IG. (Right) (a)–(d) ER-HDX of the b_2 ion from NAAIG, NA(Abu)IG, NAVIG, and NA(tbG)IG, respectively. * Due to laser failure, action IRMPD spectrum was acquired in two segments. A similar series of spectra, obtained using higher-energy source conditions, is shown in ESI Fig. S3.†

side chain of the third residue is sequentially increased from a methyl group (A), to an ethyl (Abu), to an isopropyl (V), to a *tert*-butyl (tbG), the NH_2 scissoring mode of the oxazolone (1690 cm^{-1}), the most dominant band in the oxazolone spectrum, can be seen to increase in intensity. More bulk in the side chain of the third residue thus shifts the b_2 population towards the oxazolone structure. However, because action IRMPD is known to be poorly suited to estimating relative population abundances of isomers, gas phase HDX following activation of the precursor peptide at different collision energies (ER-HDX) was performed on the b_2 populations of the four NAXIG analogues, and is shown in the right panel of Fig. 4. A single population, centered at D_0, is observed for the b_2 from NAAIG and NA(Abu)IG. In contrast, at least two distinct populations are observed in the HDX distributions of the b_2 ions from NAVIG and NA(tbG)IG, one dominated by D_0, and a second centered at D_2. Although the oxazolone and the diketopiperazine structures both have 5 exchangeable protons, the slow exchanging population can be assigned to the diketopiperazine because all five of the protons are amide protons, which are known to exchange more slowly than the protons from acidic or basic groups[20,23,38] In contrast, the oxazolone structure contains two amide protons, two amine protons, and one imine proton; thus, it is expected to rapidly exchange 2–3 protons with ND_3, consistent with the second population. HDX is therefore in excellent agreement with the action IRMPD data, in which the NA b_2 population from NAAIG and NA(Abu)IG appeared to be dominantly diketopiperazine, and a mixture of oxazolone and diketopiperazine when generated from NAVIG and NA(tbG)IG.

In order to understand the how energy impacts the formation of the diketopiperazine and oxazolone structures, it is necessary to examine the ER-HDX data for each analogue. HDX spectra were collected in triplicate and these data are summarized in Fig. 5 as a function of diketopiperazine abundance (see Fig. 4 for representative exchange patterns). The population abundance of the oxazolone and diketopiperazine isomers was estimated by fitting the HDX distribution to Poisson functions and manually parameterizing the fits. Typical variances for these fits were less than 0.001. This approximation is by no means an exact representation of the oxazolone and diketopiperazine populations, but is useful for tracking relative abundance of the two populations as a function of collision energy. With the exception of the b_2 from NAA, all b_2 populations exhibit a decrease in diketopiperazine abundance (and therefore an increase in oxazolone abundance) as collision energy is increased. The increase in b_2 diketopiperazine abundance in the NAA system clearly indicates that the energetics of the oxazolone and diketopiperazine pathways are different in the tripeptide analogue compared with the pentapeptide analogues. The b_2 diketopiperazine abundance as a function of energy can be well fit to parabolic functions, with NAAIG and NA(Abu)IG having convex curvature and NAVIG and NA(tbG)IG having a concave curvature. This curvature is interesting and may be a reflection of the interplay of enthalpy and entropy, but because the full thermodynamics of these transition states are not known, it is difficult to say with any certainty why the curvature is present. It is interesting to the note the change in behavior of the b_2 population as the side chain of the third residue is changed from an ethyl group to an isopropyl (Abu to V), as the slope and curvature of the b_2 diketopiperazine abundance *versus* energy relationship dramatically changes between these residues. This behavior suggests that the structure and shape of the isopropyl side chain is particularly significant to the energy barriers along the oxazolone and

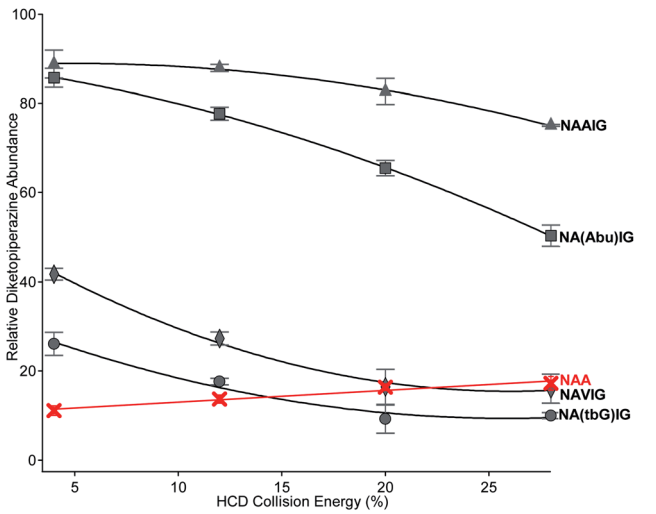

Fig. 5 Relative abundance of the b_2 diketopiperazine population from NAAIG (triangles), NA(Abu)IG (squares), NAVIG (diamonds), NA(tbG)IG (circles), and NAA (Xs) as a function of the HCD collision energy used to generate the b_2 population.

diketopiperazine pathways, and that the presence of branching groups plays a particularly important role in these pathways.

The observed decrease in diketopiperazine abundance as a function of increasing collision energy is unusual because the diketopiperazine structure is calculated to be 51.5 kJ mol^{-1} lower in energy than the oxazolone structure. In addition, the ring closure and dissociation barriers of the diketopiperazine from GG and GGG have been shown to be significantly higher than these barriers for the oxazolone structure.[15,18] Thus, the diketopiperazine structure is typically thought to be the thermodynamic product and form at higher collision energies than the oxazolone, even though the energetic difference between the two structures is relatively small. This line of reasoning seems to support the data for the NAA system, in which slightly more diketopiperazine (≈5% increase) seems to form at the highest collision energies. One explanation for more abundant diketopiperazine at low energies in the pentapeptide systems is that the oxazolone structure is entropically favored over the diketopiperazine due to the differences in closing a five *vs.* a six membered ring. In terms of transition state barriers, this suggests that the highest barrier to the formation of the diketopiperazine, be it ring closure, *trans–cis* isomerization, or dissociation, must be lower in energy than the highest energy barrier for the formation of the oxazolone structure, presumably the ring closure barrier. However, because closure of a five-membered ring is more entropically favorable, the oxazolone ring closure transition state must be looser than the diketopiperazine transition state; the density of states at these saddle points therefore allows oxazolone formation to be competitive with diketopiperazine formation at high collision energies. Fig. 6 shows a diagram describing this reasoning.

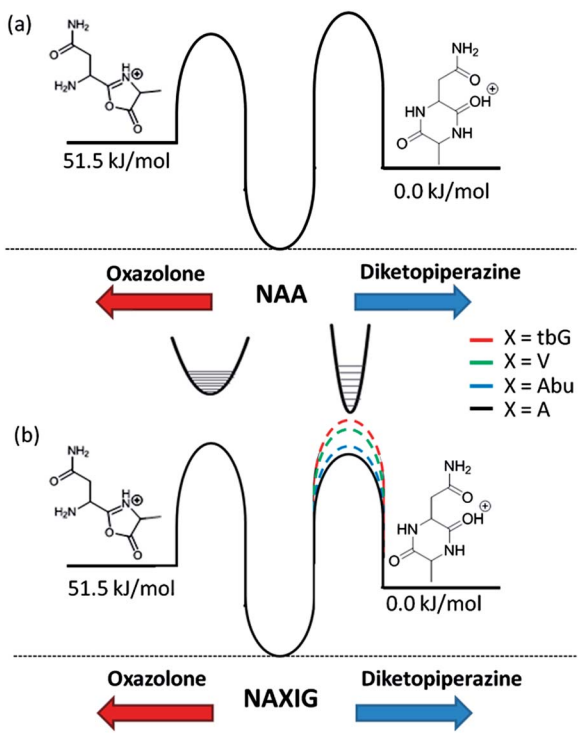

Fig. 6 Diagram showing estimated ring closure barriers for the formation of oxazolone and diketopiperazine b_2 ion structures for (a) NAA and (b) NAXIG based on ER-HDX data and computational modeling of NA b_2 oxazolone and diketopiperazine structures.

It is clear from an energetic perspective that the relative energies and tightness of the oxazolone and diketopiperazine transition states play a critical role in favoring oxazolone or diketopiperazine formation. However, the direct role of the side chain of the third residue in the peptide system on the relative energies of these barriers is less obvious. It is appealing to consider this problem in terms of backbone rotational freedom, as the more bulky side chains undoubtedly limit the rotational space of the backbone psi and phi dihedral angles. From this perspective, it is straightforward to propose a mechanism in which the more bulky side chains, that is, valine and *tert*-butyl glycine, restrict backbone torsional angles such that certain proton bridges are disfavored or altogether impossible. It is possible that the absence or presence of such interactions would favor or disfavor certain fragmentation pathways. However, the precise interactions, particularly those related to the *trans–cis* isomerization and ring closure transition states, require extensive computational modeling of the precursor peptides and fragmentation intermediates such as the b_4 ion and is beyond the scope of this paper. Nonetheless, it is clear that peptide composition and length play a significant role in the formation of b_2 fragment ion structures in systems containing an N-terminal asparagine.

Conclusions

Action IRMPD of the b_2 population of NAA, NAAIG, NA(Abu)IG, NAVIG, and NA(tbG)IG shows the presence of at least two isomeric b_2 structures. Action IRMPD of the b_2-NH_3 from the b_2 of NAAIG and computational modeling allow these two structures to be assigned as a ring protonated oxazolone and a ring carbonyl oxygen protonated diketopiperazine. This is the first instance of diketopiperazine formation in a peptide without a basic residue or a proline. Moreover, the bulk of the third residue and peptide length are additionally shown for the first time to be factors in oxazolone *vs.* diketopiperazine formation. Energy resolved HDX suggests that the relative energy and tightness of the oxazolone and diketopiperazine transition states are critical factors along these two pathways. Changes in trendlines relating diketopiperazine abundance to collision energy suggests the presence of a branching group in the third position of the pentapeptide causes the oxazolone pathway to be favored. This is in direct contrast to the pentapeptide systems containing only a methyl or an ethyl group in this position, as these analogues strongly favor the diketopiperazine structure. A systematic study varying the length and chemical identity of the first and third residues and more extensive modeling of transition states is necessary to more fully understand the mechanistic details of this behavior.

Acknowledgements

Professor Anne McCoy is acknowledged for her assistance in interpreting multi-photon effects in the action IRMPD spectra. This research is supported by NIH R01 51387 to Dr Wysocki and

Ohio State University. The authors thank the CLIO team (J. M. Ortega, C. Six, G. Perilhous, J. P. Berthet) as well as P. Maître and V. Steinmetz for their support during the experiments. The research leading to these results has received funding from the European Union's Seventh Framework Program (FP7/2007-2013) under grant agreement number 226716.

Notes and references

1 H. V. Florance, A. P. Stopford, J. M. Kalapothakis, B. J. McCullough, A. Bretherick and P. E. Barran, *Analyst*, 2011, **136**, 3446.
2 M. F. Jarrold, *Phys. Chem. Chem. Phys.*, 2007, **9**, 1659.
3 H. Oh, K. Breuker, S. K. Sze, Y. Ge, B. K. Carpenter and F. W. McLafferty, *Proc. Natl. Acad. Sci. U. S. A.*, 2002, **99**, 15863.
4 C. Bleiholder, N. F. Dupuis, T. Wyttenbach and M. T. Bowers, *Nat. Chem.*, 2011, **3**, 172.
5 V. Katta and B. T. Chait, *J. Am. Chem. Soc.*, 1991, **113**, 8534.
6 M. Sharon, *J. Am. Soc. Mass Spectrom.*, 2010, **21**, 487.
7 T. Taverner, H. Hernandez, M. Sharon, B. T. Ruotolo, D. Matak-Vinkovic, D. Devos, R. B. Russell and C. V. Robinson, *Acc. Chem. Res.*, 2008, **41**, 617.
8 A. V. Tolmachev, E. W. Robinson, S. Wu, L. Pasa-Tolic and R. D. Smith, *Int. J. Mass Spectrom.*, 2009, **287**, 32.
9 M. Zhou, C. Huang and V. H. Wysocki, *Anal. Chem.*, 2012, **84**, 6016.
10 D. M. Wardlaw and R. A. Marcus, *Chem. Phys. Lett.*, 1984, **110**, 230.
11 L. L. Griffin and D. J. McAdoo, *J. Am. Soc. Mass Spectrom.*, 1993, **4**, 11.
12 B. Paizs and S. Suhai, *Mass Spectrom. Rev.*, 2005, 508.
13 B. R. Perkins, J. Chamot-Rooke, S. H. Yoon, A. C. Gucinski, A. Somogyi and V. H. Wysocki, *J. Am. Chem. Soc.*, 2009, 17528.
14 B. Balta, V. Aviyente and C. Lifshitz, *J. Am. Soc. Mass Spectrom.*, 2003, **14**, 1192.
15 P. B. Armentrout and A. L. Heaton, *J. Am. Soc. Mass Spectrom.*, 2012, **23**, 632.
16 T. Yalcin, I. G. Csizmadia, M. R. Peterson and A. G. Harrison, *J. Am. Soc. Mass Spectrom.*, 1996, **7**, 233.
17 N. C. Polfer, J. Oomens, S. Suhai and B. Paizs, *J. Am. Chem. Soc.*, 2005, **127**, 17154.
18 B. Paizs and S. Suhai, *Rapid Commun. Mass Spectrom.*, 2002, **16**, 375.
19 M. J. Nold, C. Wesdemiotis, T. Yalcin and A. G. Harrison, *Int. J. Mass Spectrom. Ion Processes*, 1997, **164**, 137.
20 A. C. Gucinski, J. Chamot-Rooke, E. Nicol, A. Somogyi and V. H. Wysocki, *J. Phys. Chem. A*, 2012, **116**, 4296.
21 J. M. Farrugia, T. Taverner and R. A. J. O'Hair, *Int. J. Mass Spectrom.*, 2001, **209**, 99.
22 L. L. Smith, K. A. Herrmann and V. H. Wysocki, *J. Am. Soc. Mass Spectrom.*, 2006, **17**, 20.
23 A. C. Gucinski, J. Chamot-Rooke, V. Steinmetz, A. Somogyi and V. H. Wysocki, *J. Phys. Chem. A*, 2013, **117**, 1291.
24 S. Zou, J. Oomens and N. C. Polfer, *Int. J. Mass Spectrom.*, 2012, **316–318**, 12.
25 J. Oomens, S. Young, S. Molesworth and M. van Stipdonk, *J. Am. Soc. Mass Spectrom.*, 2009, **20**, 334.
26 B. Bythell, Á. Somogyi and B. Paizs, *J. Am. Soc. Mass Spectrom.*, 2009, **20**, 618.
27 S. H. Yoon, J. Chamot-Rooke, B. R. Perkins, A. E. Hilderbrand, J. C. Poutsma and V. H. Wysocki, *J. Am. Chem. Soc.*, 2008, **130**, 17644.
28 G. Bouchoux, *Mass Spectrom. Rev.*, 2012, **31**, 391.
29 *Solid-Phase Peptide Synthesis: A Practical Approach*, ed. E. Atherton and R. C. Sheppard, Oxford University Press, Oxford, 1989.
30 J. V. Olsen, B. Macek, O. Lange, A. Makarov, S. Horning and M. Mann, *Nat. Methods*, 2007, **4**, 709.
31 A. Simon, W. Jones, J.-M. Ortega, P. Boissel, J. Lemaire and P. Maitre, *J. Am. Chem. Soc.*, 2004, **126**, 11666.
32 P. Maître, S. Le Caër, A. Simon, W. Jones, J. Lemaire, H. Mestdagh, M. Heninger, G. Mauclaire, P. Boissel, R. Prazeres, F. Glotin and J.-M. Ortega, *Nucl. Instrum. Methods Phys. Res., Sect. A*, 2003, **507**, 541.
33 M. J. Frisch G. W. Trucks; H. B. Schlegel, G. E. Scuseria, M. A. Robb, J. R. Cheeseman, G. Scalmani, V. Barone, B. Mennucci, G. A. Petersson, H. Nakatsuji, M. Caricato, X. Li, H. P. Hratchian, A. F. Izmaylov, J. Bloino, G. Zheng, J. L. Sonnenberg, M. Hada, M. Ehara, K. Toyota, R. Fukuda, J. Hasegawa, M. Ishida, T. Nakajima, Y. Honda, O. Kitao, H. Nakai, T. Vreven, J. A. Montgomery, Jr, J. E. Peralta, F. Ogliaro, M. Bearpark, J. J. Heyd, E. Brothers, K. N. Kudin, V. N. Staroverov, R. Kobayashi, J. Normand, K. Raghavachari, A. Rendell, J. C. Burant, S. S. Iyengar, J. Tomasi, M. Cossi, N. Rega, J. M. Millam, M. Klene, J. E. Knox, J. B. Cross, V. Bakken, C. Adamo, J. Jaramillo, R. Gomperts, R. E. Stratmann, O. Yazyev, A. J. Austin, R. Cammi, C. Pomelli, J. W. Ochterski, R. L. Martin, K. Morokuma, V. G. Zakrzewski, G. A. Voth, P. Salvador, J. J. Dannenberg, S. Dapprich, A. D. Daniels, Ö. Farkas, J. B. Foresman, J. V. Ortiz, J. Cioslowski and D. J. Fox, *Gaussian, I., 09 ed.*, Wallingford, CT, 2009.
34 L. Schrödinger, *MacroModel, version 10.2*, New York, NY, 9.9 edn, 2011.
35 B. Godugu, P. Neta, Y. Simon-Manso and S. E. Stein, *J. Am. Soc. Mass Spectrom.*, 2010, **21**, 1169.
36 P. Neta, Q.-L. Pu, L. Kilpatrick, X. Yang and S. E. Stein, *J. Am. Soc. Mass Spectrom.*, 2007, **18**, 27.
37 J. Grzetic and J. Oomens, *J. Am. Soc. Mass Spectrom.*, 2013, **24**, 1228.
38 J. Pan, B. L. Heath, R. A. Jockusch and L. Konermann, *Anal. Chem.*, 2012, **84**, 373.